Probabilistic Model for Flexural Strength of Carbon Nanotube Reinforced Cement-based Materials

Mahyar Ramezani, Young Hoon Kim*, and Zhihui Sun

Department of Civil and Environmental Engineering, University of Louisville, Louisville, KY 40292, USA

Mahyar Ramezani

E-mail: mahyar.ramezani@louisville.edu

Young Hoon Kim

* Corresponding author

Tel: 502-852-4565

E-mail: young.kim@louisville.edu

Zhihui Sun

E-mail: z.sun@louisville.edu

Probabilistic Model for Flexural Strength of Carbon Nanotube Reinforced Cement-based Materials

Mahyar Ramezani, Young Hoon Kim*, and Zhihui Sun

Abstract: The bond between carbon nanotubes (CNTs) and cementitious materials is the key characteristic for predicting the flexural strength. However, CNT dispersion quality dominantly changes the bonding mechanism. A probabilistic approach can benefit analytical models to capture various sources of uncertainty affecting the dispersion and bonding characteristics. This study proposes a probabilistic model based on the deterministic Kelly-Tyson theory to predict the flexural strength of CNT reinforced cementitious composites. The proposed probabilistic model considers the contributions of multiple experimental variables to CNT dispersion quality, bonding mechanism and the flexural strength. To this end, a Bayesian methodology is employed to calibrate the unknown model parameters and various sources of uncertainty using extensive experimental test data from the literature including the authors' work. The developed probabilistic model is then used to identify the optimum ranges of each variable to maximize the flexural strength through computing the failure probability which is defined as the probability of not meeting certain flexural strength requirements (herein, 50% increase compared with the control). Finally, the effect of changes in different variables on the probability estimates is examined using sensitivity and importance measures. The analysis reveals that the proposed model can capture the experimentally observed trends for predicting the flexural strength with reasonable accuracy.

Keywords: Carbon nanotubes; Cementitious composites; Flexural strength; Dispersion; Interfacial bond strength; Kelly-Tyson model; Bayesian methodology; Probabilistic model

1. Introduction

Concrete cracks when subjected to tensile forces. Over the past decades, various types of fibers (steel or synthetic) have been used to compensate for the low tensile/flexural strength of concrete by mitigating the crack propagation [1, 2]. The contributions of fibers to delay the crack propagation rely on the shape and size of the fibers, their surface textures and the interfacial bond strength between the fibers and the matrix [3, 4]. In this regard, incorporating smaller fibers might help to delay the initiation of cracks [5]. Recently, carbon nanotubes (CNTs) have been extensively used to increase the flexural strength of cementitious composites (cement paste, cement mortar and concrete) [6, 7]. The nanoscale size of CNTs reduces the distance between adjacent nanotubes, delaying the crack propagation. Also, CNTs have tensile strength of around 30 *GPa* with elastic modulus in the range of 1 *TPa* [8, 9]. Because of the extraordinary physical and mechanical properties of CNTs, many studies have reported that the flexural strength of CNT reinforced cementitious composites has been increased significantly [6, 7, 10, 11]. However, the authors' statistical analysis reported inconsistent results in the flexural strength of cementitious materials reinforced with CNTs (herein, CNT-cement composites) [5]. The discrepancy can be attributed to the CNT dispersion and bonding states within the cement matrix [12, 13]. The bond strength between CNTs and the cement matrix is dominantly governed by CNT dispersion quality [14]. The dispersion quality, itself, depends on multiple factors such as physical characteristics of CNTs, dispersion procedure and cement matrix composition. The improper combinations of these factors often lead to degradation of the interfacial bond and flexural strengths. To address this, an analytical model can be a viable option to estimate the bond strength between CNTs and the matrix considering the contributions of multiple experimental variables for maximizing the flexural strength of CNT-cement composites.

Recently, various analytical models considering CNT physical characteristics (e.g., length, diameter and volume fraction) have been used to predict the tensile strength of polymers, metals and ceramics [15, 16]. For example, the interfacial bond strength of CNTs in a metal matrix was increased when using longer CNTs, resulting in higher tensile strength [15]. The agglomeration of CNTs, however, reduced the frictional forces resulting in debonding from the metallic matrix [17]. Although the interfacial bond strength is very critical in determining the tensile/flexural strength [18], the existing models (e.g., Halpin-Tsai model [19] and Kelly-Tyson model [20]) typically assume a homogenous dispersion and perfect bond between CNTs and the hosting matrix [21]. Therefore, few researchers have modified the existing models by adding a multiplier of dispersion coefficient [22-24]. The different dispersion mechanism of CNTs in cement matrix, however, limits the applicability of the existing models to CNT-cement composites. The dispersion coefficient should therefore be formulated by parameters such as the CNT physical characteristics, dispersion procedure and matrix composition. Recently, the literature data was analyzed to identify the most important variables and their interactions affecting the dispersion quality, bond strength and the flexural strength [5]. The influence of CNTs on the rate of cement hydration is another important variable affecting the flexural strength that needs to be considered in the prediction model [5, 14].

This study aims to propose a reliable model to understand the effects of CNT dispersion, bond strength and cement hydration process on the flexural strength of cementitious composites (pastes and mortars). The following section presents the base model (Kelly-Tyson model [20]) and the required modifications in order to improve its predictability for CNT-cement composites. Besides, because incorporating CNTs is correlated with a high degree of uncertainty, a probabilistic approach is adopted to consider various sources of uncertainty to affect the flexural strength. Using existing experimental test data obtained from the literature, several probabilistic models are developed and the best model is selected. Then, the performance of the proposed model is evaluated using the reliability analysis. The proposed model in this study can explain the reported experimental trends in the literature including the contradictory test results and provide valuable information for future researcheres and designers to identify the best combination of the experimental variables to achieve certain performance.

2. Modified Kelly-Tyson Model

The Kelly-Tyson model [20] which is the extension of the well-known rule of mixtures has been extensively used to predict the tensile strength of brittle and ductile materials containing CNTs such as polymers, metals and ceramics [16, 25-28]. Besides, the Kelly-Tyson model was used to predict the flexural strength of concrete reinforced with short discrete fibers [29, 30]. For condition of equal elastic strain in the fiber and matrix, the rule of mixtures is considered as the simplest way to model the tensile strength of composites reinforced with aligned continuous fibers [31]:

$$\sigma_c = \sigma_f v_f + \sigma_m (1 - v_f) \tag{1}$$

where σ_c is the ultimate tensile strength of the composite (*MPa* or *psi*), σ_f is the tensile strength of the fiber (*MPa* or *psi*), σ_m is the tensile strength of the matrix at ultimate strain of the composite (*MPa* or *psi*) and v_f is the volume fraction of the fiber (unitless). To consider the contribution of the semi-aligned short discrete fibers, Eq. (1) can be modified to include the fiber length (χ_L) and orientation (χ_o) factors. To account for the randomness in fiber orientations, the χ_o can be calculated as $\chi_o = \sum_n a_n \cos^4 \Phi_n$ where a_n is the fraction of fibers having the orientation angle Φ_n with respect to the reference axis [32]. When using aligned fibers, the value of χ_o is one and it is equal to 3/8 and 1/6 for randomly orientated fibers in two and three dimensions, respectively

[33]. Due to the extremely small sizes of CNTs, they are assumed to be randomly arranged in three dimensions (i.e., $\chi_o = 1/6$) [22, 23].

Kelly and Tyson [20] have developed the χ_L for fibers having lengths (L) shorter or longer than the fiber critical length ($L_c = {\sigma_f d}/{2\tau_i}$; d is the fiber diameter and τ_i is the interfacial bond stress) to determine the mode of failure: fiber fracture ($L \geq L_c$) or pull-out ($L < L_c$). Therefore, the tensile strength of composites can be calculated as follows:

$$\sigma_c = \chi_o \left[\sum_{L=0}^{L<L_c} \tau_i \left(\frac{L}{d}\right) + \sum_{L=L_c}^{L} \left(1 - \frac{L_c}{2L}\right) \sigma_f \right] v_f + \sigma_m (1 - v_f) \tag{2}$$

where the first and second terms in the bracket are contributions from fibers with $L < L_c$ and $L \geq L_c$, respectively. Because CNT length in cementitious composites is generally smaller than the critical length ($L < L_c$), the contribution of CNTs with $L \geq L_c$ is neglected.

Also, due to the very low volume fraction of CNTs used in cementitious materials ($v_f =$ 0.00004-0.00128; based on the database), the predicted flexural strength of CNT-cement nanocomposites using Eq. (2) is almost the same as the flexural strength of the matrix. The authors' preliminary study has shown that ${v_f}^{2/3}$ is appropriate to fit the experimental data. The modified form of the Kelly-Tyson equation to predict the flexural strength of CNT-reinforced cementitious composites can therefore be expressed as follows:

$$\sigma_c = {1}/{6}\, \tau_i (AR) {v_f}^{2/3} + \sigma_m \left(1 - {v_f}^{2/3}\right) \tag{3}$$

where AR is CNT aspect ratio ($AR = {L}/{d}$). To predict the flexural strength using Eq. (3), τ_i must be quantified. The experimental investigations to measure τ_i is challenging or impractical due to the limitations associated with nanoscale sizes. Therefore, theoretical approaches might be used to determine the interface properties [34]. In this study, the Pukanszky model [35] is used to correlate the composite strength with the interface properties. Note that Pukanszky model have been widely used to characterize the composites containing various nanoparticles including nanoclays, layered silica nanoparticles and CNTs [16, 36, 37]:

$$\sigma_c = \sigma_m(\frac{1 - {v_f}^{2/3}}{1 + 2.5\, {v_f}^{2/3}})e^{B{v_f}^{2/3}} \tag{4}$$

where B is the empirical adhesion parameter that reflects the capacity of stress transfer between CNTs and matrix. In this study, B is calculated using the available experimental data from the literature including the authors' work. According to Lazzeri and Phuong [38], the adhesion parameter B can be correlated with τ_i in the Kelly-Tyson model. Therefore, in this study, τ_i is attained by connections between Eqs. (3) and (4):

$$\tau_i = \frac{6\sigma_m(B - 2.5)}{AR} \tag{5}$$

To calculate τ_i for each individual data, the average value of B for the entire dataset ($B_{avg} = 55$) is used as the representative value for adhesion between CNTs and cement matrix. The statistics of B and τ_i are shown in Table 1.

Table 1. Statistics of the Pukanszky adhesion parameter (B) and interfacial bond stress (τ_i)

Parameter	Minimum	Maximum	Mean	Median	Standard deviation
***B* (unitless)**	-7.827	255.9	54.92	44.19	43.85
τ_i (*MPa*)	0.63	9.28	2.98	1.97	2.27

2.1.Critical Factors Affecting CNT Mechanisms in Cementitious Composites

To understand the mechanisms of CNTs within cementitious materials (e.g., bonding, dispersion and cement hydration rate mechanisms), three critical factors were proposed in the authors' previous work [14] to capture the interactions between the important experimental variables to predict the mechanical properties including the flexural strength.

1) dispersion factor (η_D) to correlate CNT dispersion as a functions of *AR*, CNT volume fraction in aqueous solution (v_{f-w}), superplasticizer-to-CNTs (*SP/CNTs*) ratio and Ultrasonication Energy Indicator (*UEI*)
2) matrix factor (η_M) to include the influence of water-to-cement ratio (*w/c*) and sand-to-cement ratio (*s/c*)
3) hydration age factor (η_H) to consider the interactions between CNT concentration (κ) and hydration age of cement (*t*)

A brief description of these critical factors is provided in Table 2. More details are provided in the authors' previous study [14]. The applicability of the proposed critical factors to predict the flexural strength is validated in Section 5.1.

Table 2. Critical factors affecting the flexural strength

Critical factor	Equation	Variable (unit)	Mechanism
η_D	$1-\left[\frac{AR}{UEI}\times\frac{v_{f-w}}{(SP/_{CNTs})}\right]$	AR = CNT aspect ratio (unitless) v_{f-w} = CNT volume fraction in aqueous solution (unitless) UEI = ultrasonication energy indicator (index, express in minute) $SP/_{CNTs}$ = superplasticizer-to-CNTs ratio (unitless)	If v_{f-w} or AR = 0 (i.e., no CNTs added), η_D = 1 (i.e., perfect dispersion). As v_{f-w} and/or AR increases, η_D gets smaller. As *UEI* and/or $SP/_{CNTs}$ increases, η_D gradually reaches one. Beyond certain *UEI* and/or $SP/_{CNTs}$, η_D gets constant.
η_M	$\frac{(1+{}^{s}/_{c})}{({}^{w}/_{c})}$	${}^{s}/_{c}$ = sand-to-cemet ratio (unitless) ${}^{w}/_{c}$ = water-to-cement ratio (unitless)	As *w/c* ratio decreases, the value of η_M increases. As *s/c* ratio increases, the value of η_M increases.
η_H	$\left(\frac{t}{4+0.85t}\right)^{\kappa}$	t = age of specimen (days) κ = CNT concentration (*c-wt*%)	If CNT is not added (κ = 0 *c-wt*%), η_H = 1. At low CNT concentrations (κ ≤ 0.1 *c-wt*%), the influence of *t* on η_H is minimal. As κ increases, η_H reaches unity (η_H = 1) at later ages (i.e., the higher value of *t*).

Note: η_D: dispersion factor; η_M: matrix factor; η_H: hydration age factor

To correct the bias in Eq. (3) and to capture the mechanisms of CNTs in cementitious materials, the proposed critical factors (η_D, η_H and η_M) are added to the modified form of the Kelly-Tyson model as follows:

$$\sigma_c = \eta_D\eta_H\eta_M\left[{}^{1}/_{6}\,\tau_i(AR)v_f{}^{2/3} + \sigma_m\left(1 - v_f{}^{2/3}\right)\right] \quad (6)$$

In addition, Eq. (6) is formulated in a probabilistic manner using a Bayesian methodology to consider different sources of uncertainty such as the statistical uncertainty in the estimation of the unknown model parameters, the model errors associated with the inaccurate form of the model and missing variables [39] that might influence the flexural strength.

3. Formulation of the Probabilistic Model

To formulate the modified form of the deterministic Kelly-Tyson model (see Eq. (6)) in a probabilistic manner, additional correction terms (herein, η_D, η_H and η_M) and model error are added to the deterministic expression to account for the inherent bias and to capture the remaining variability in residuals, respectively [39]. The probabilistic model relates the quantity of interest (herein, the flexural strength; σ_c) to a set of measurable variables (defined as $\boldsymbol{x} = (x_1, x_2, x_3, \ldots)$) such as *AR*, κ, *UEI*, *SP/CNTs* ratio, *w/c* ratio, *s/c* ratio, *t*, etc. The probabilistic capacity model can be written as follows:

$$C(\boldsymbol{x}, \boldsymbol{\Theta}) = C(\boldsymbol{x}) + \gamma(x, \Theta) + \partial\varepsilon \tag{7}$$

where $C(\boldsymbol{x}, \boldsymbol{\Theta})$ is the capacity model of interest (herein, σ_c), $\boldsymbol{x}$ is a set of measurable variables, $\boldsymbol{\Theta} = (\theta, \sigma)$, $\theta = (\theta_1, \theta_2, \theta_3, \ldots)$ denotes a set of unknown model parameters used to fit the data, $C(\boldsymbol{x})$ is the selected deterministic model, $\gamma(x, \theta)$ is the correction term (herein, η_D, η_H and η_M), ∂ is a standard deviation of the error term taken from Var $[C(\boldsymbol{x}, \boldsymbol{\Theta})] = \partial^2$, ε is a random variable with zero mean and unit variance and $\partial\varepsilon$ is the error term of the model. The final form of the probabilistic model used to predict the flexural strength of CNT-cement composites is as follows:

$$\sigma_c = \eta_D(x_D, \theta_D) \times \eta_H(x_H, \theta_H) \times \eta_M(x_M, \theta_M) \times \left[1/6\tau_i(AR){v_{f-m}}^{2/3} + \sigma_m\left(1 - {v_{f-m}}^{2/3}\right)\right] + \partial\varepsilon \tag{8}$$

where v_{f-m} is the volume fraction of CNTs within the cement matrix and $\theta = (\theta_D, \theta_H, \theta_M)$ are unknown model parameters used to fit the data: $\eta_D(x_D, \theta_D) = \left[1 - \left(\frac{AR^{\theta_1} \times v_{f-w}{}^{\theta_3}}{UEI^{\theta_2} \times \left({SP}/{CNTs}\right)^{\theta_4}}\right)\right]$, $\eta_H(x_H, \theta_H) = \left(\frac{t}{4+0.85t}\right)^{\kappa\theta_5}$, and $\eta_M(x_M, \theta_M) = \frac{(1+{S}/{C})^{\theta_6}}{({W}/{C})^{\theta_7}}$.

3.1. Bayesian Parameter Estimation

To calibrate the unknown model parameters, a Bayesian updating rule [40] is used because it allows to update their statistics (i.e., means, variances and correlation coefficient) as new data becomes available in the future [41]:

$$f(\boldsymbol{\Theta}) = \lambda L(\boldsymbol{\Theta}) p(\boldsymbol{\Theta}) \tag{9}$$

where $\boldsymbol{\Theta}$ is a vector of unknown model parameters, $p(\boldsymbol{\Theta})$ is prior distribution of $\boldsymbol{\Theta}$ based on the knowledge about $\boldsymbol{\Theta}$ that represents the information available before collecting the data *Đ* of size *n*, $L(\boldsymbol{\Theta})$ is the likelihood function that captures the information on $\boldsymbol{\Theta}$ from data *Đ* which is proportional to the conditional probability $P(Đ|\boldsymbol{\Theta})$ of observing *Đ* for given values of $\boldsymbol{\Theta}$, $\lambda = [\int L(\boldsymbol{\Theta}) p(\boldsymbol{\Theta})\, d(\boldsymbol{\Theta})]^{-1}$ is a normalizing factor, and $f(\boldsymbol{\Theta})$ is posterior distribution that shows the updated state of information about $\boldsymbol{\Theta}$. Once $f(\boldsymbol{\Theta})$ is known, the posterior mean vector ($M_{\boldsymbol{\Theta}}$) and the covariance matrix ($\Sigma_{\boldsymbol{\Theta\Theta}}$) are obtained. Because there is no prior information about $\boldsymbol{\Theta}$ is available before collecting data *Đ,* a non-informative prior distribution is assumed [39]. If new data becomes available in the future, Eq. (9) can still be used to update the estimates of the unknown model parameters by using the current $f(\boldsymbol{\Theta})$ as a new previous distribution.

4. Database

A total of 105 data is collected from several literatures including the authors' work [6, 10, 14, 42-48] to calibrate the unknown model parameters in Eq. (8) using a Bayesian methodology. To evaluate the robustness of the proposed probabilistic model, the database is split into two sets of data (training set and test set) using a hold-out method [49]. This process minimizes the issues of overfitting and being overly optimistic on model error [50]. The training set is used to estimate the unknown model parameters and the test set is used to evaluate the performance of the developed model. The training set is selected using a random subsampling method without replacement [49]. Besides, two different random selections of *A* and *B* are provided. The two different random selections is to ensure that more data get a chance to be the test set, resulting in an unbiased evaluation of the model performance. In both random selections, 80% of the data (training set; 84 data points) is used to develop the model (datasets I and III for random selections *A* and *B*, respectively) and the remaining 20% of the data (test set; 21 data points) is used to validate the model (datasets II and IV for random selections *A* and *B*, respectively).

Table 3 shows the minimum, maximum, mean, median and standard deviation of different variables used to develop the probabilistic model (random selection *A*: dataset I). The average values of *L*, *d* and *AR* are used. For example, if *L* and *d* are reported to be between 10-30 μm and 20-40 *nm*, respectively, then average length, diameter, and aspect ratio of 20 μm, 30 *nm* and 667 (unitless) are used.

Table 3. Range of Variables to Develop Probabilistic Model (random selection *A*: dataset I)

Variables	Minimum	Maximum	Mean	Median	Standard deviation
κ (*c-wt%*)	0.0125	0.5	0.1033	0.09	0.0987
L (μm)	1.5	55	21.7	20	13.45
d (nm)	8	32.5	25.29	27.5	7.58
AR (unitless)	157.89	2500	902.83	800	622.28
SP/CNTs	1.32	24	6.4	4	5.26
w/c	0.3	0.6	0.426	0.45	0.0748
s/c	0	3	1.527	2.25	1.235
Age (days)	3	28	14.643	7	11.18
σ_m(*MPa*)	1.94	9.3	5.36	4.88	1.91
UE_t (*J/ml*)	25	2800	1703.65	2612.5	1208.2
UE_m (*J/ml/min*)	3.95	28	9.21	8	5.998
UA (%)	30	100	55.63	50	15.63

5. Probabilistic Model Assessment

Tables 4 and 5 show the posterior statistics of $\mathbf{\Theta}$ estimated using dataset I (for random selection A) and dataset III (for random selection B). The mean values of the unknown model parameters for datasets I and III differs from one another by less than 20% (except for θ_{5A} and θ_{5B} which exhibit 22.1% difference). This indicates the robustness of the proposed model. Besides, the accuracy of the proposed probabilistic model is evaluated as shown in Fig. 1. The solid circles are the datasets I and III used to develop the model and the open triangles are the datasets II and IV used to validate the model. The predicted flexural strength for most of the data shows good accuracy within the solid lines (i.e., within ± standard deviation of the error term in the proposed model; ∂_A = 15% and ∂_B = 18%). The robustness of the proposed probabilistic model can be validated using datasets II and IV (open triangles) that are not used for the estimation of the unknown model parameters. Note that the three data points inside the oval in Fig. 1 (a) and (b) are related to the flexural strength of cement mortar reinforced with mechanical functionalized CNTs at different ages (3, 7 and 28 days). The mechanical functionalized CNTs provided superior bond properties [6], resulted in under-prediction of the flexural strength.

Table 4. Posterior Statistics of the Unknown Model Parameters (random selection A: dataset I)

Unknown parameter	Mean	Standard deviation	Correlation matrix							
			θ_{1A}	θ_{2A}	θ_{3A}	θ_{4A}	θ_{5A}	θ_{6A}	θ_{7A}	∂_A
θ_{1A}	0.3925	0.0280	1	-0.5390	0.9981	0.9495	0.8606	-0.5683	-0.9771	0.6282
θ_{2A}	0.2798	0.0086		1	-0.5713	-0.6965	-0.6583	-0.0396	0.6082	-0.4281
θ_{3A}	0.4806	0.0299			1	0.9483	0.8541	-0.5671	-0.9786	0.6275
θ_{4A}	0.1317	0.0369				1	0.9458	-0.3876	-0.9627	0.6753
θ_{5A}	1.0589	0.0575					1	-0.2129	-0.8844	0.5981
θ_{6A}	0.1730	0.0046				Sym.		1	0.4226	-0.5294
θ_{7A}	0.1269	0.0146							1	-0.6007
∂_A	0.1491	0.0008								1

Table 5. Posterior Statistics of the Unknown Model Parameters (random selection B: dataset III)

Unknown parameter	Mean	Standard deviation	Correlation matrix							
			θ_{1B}	θ_{2B}	θ_{3B}	θ_{4B}	θ_{5B}	θ_{6B}	θ_{7B}	∂_B
θ_{1B}	0.3950	0.0876	1	0.5287	0.9739	0.4178	-0.4650	-0.4585	-0.7044	0.0411
θ_{2B}	0.3350	0.0745		1	0.4056	-0.0169	-0.1806	-0.2618	-0.5600	-0.0174
θ_{3B}	0.4751	0.0926			1	0.3769	-0.4299	-0.4915	-0.7011	0.0524
θ_{4B}	0.1055	0.0341				1	-0.2875	-0.1602	-0.4694	0.1143
θ_{5B}	0.8846	0.2263					1	0.1879	0.3906	-0.0287
θ_{6B}	0.1697	0.0255				Sym.		1	0.1756	-0.0573
θ_{7B}	0.1379	0.0555							1	-0.0903
∂_B	0.1768	0.0137								1

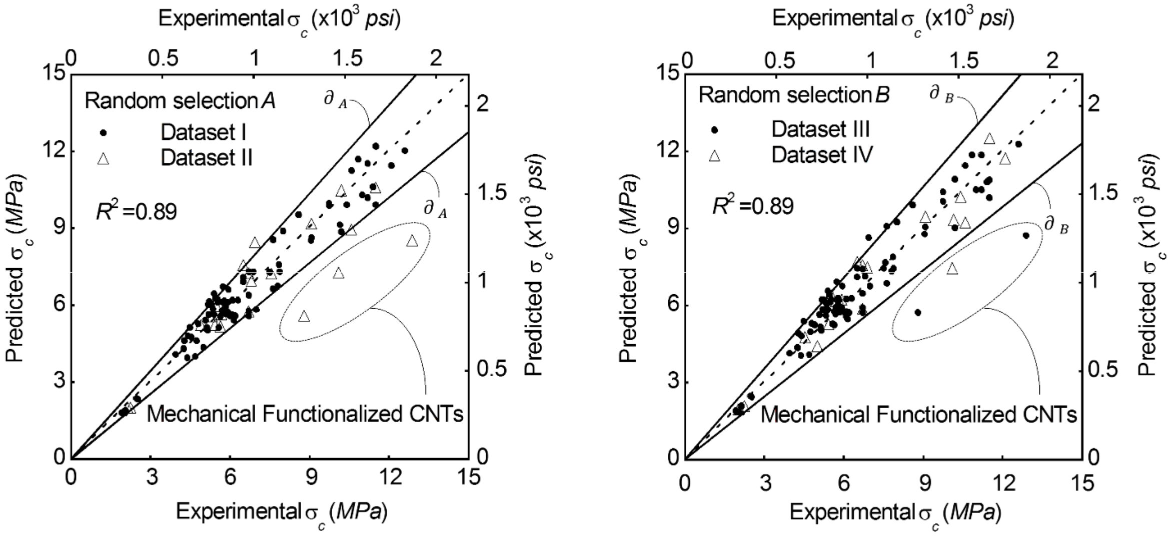

(a) (b)

Fig. 1. Predicted value of flexural strength versus experimental results (a) random selection *A* (b) random selection *B* (datasets I & III are used for model development and datasets II & IV are used for model validation)

5.1. Applicability of the Proposed Critical Factors

In this section, the corrected critical factors (i.e., $\eta_D\ (x_D, \theta_D)$, $\eta_H\ (x_H, \theta_H)$ and $\eta_M\ (x_M, \theta_M)$; see Eq. (8)) are further analyzed in order to validate their applicability to predict the flexural strength without bias. Note that because the mean values of the calibrated unknown model parameters for random selections *A* and *B* are close to one another (see Tables 4 and 5); the statistics of the unknown model parameters for random selection *A* is used for the analysis throughout this research. The proposed probabilistic model after adding the mean values of the unknown model parameters using random selection *A* is as follows:

$$\sigma_c = \left[1 - \left(\frac{AR^{0.39} \times {v_{f-w}}^{0.48}}{UEI^{0.28} \times \left({}^{SP}/_{CNTs}\right)^{0.13}}\right)\right] \times \left(\frac{t}{4 + 0.85t}\right)^{1.06\kappa} \times \frac{(1 + {}^{S}/_{C})^{0.17}}{({}^{W}/_{C})^{0.13}}$$
$$\times \left[1/6\tau_i(AR){v_{f-m}}^{2/3} + \sigma_m\left(1 - {v_{f-m}}^{2/3}\right)\right] + 0.15\varepsilon \tag{9}$$

The corrected critical factors are analyzed by comparing the estimated with the measured values. The estimated value is obtained by plugging in the value of the experimental variables in corresponding relations. For example, the estimated value of η_M (x_M, θ_M) is directly calculated using $\eta_M(x_M, \theta_M) = \left[\frac{(1+S/c)^{0.17}}{(W/c)^{0.13}}\right]$. The measured value of each critical factor is back calculated using Eq. (9) and the experimental test results of σ_c and σ_m, assuming that η_D (x_D, θ_D), η_H (x_H, θ_H) and η_M (x_M, θ_M) are not correlated.

Figs. 2 through 4 are plotted to validate the applicability of η_D (x_D, θ_D), η_H (x_H, θ_H) and η_M (x_M, θ_M), respectively. Each critical factor is plotted as a function of a main variable (*x*-axis) and its interaction with another independent variable at two different ranges: $R1$ for the experimental variable below its mean value and $R2$ for the experimental variable above the mean value (see Table 6). For example, Fig. 2 (a) shows the influence of changes in *AR* and its interaction with v_{f-w} at two different range of $R1$ $(v_{f-w} \leq 0.0012)$ and $R2$ $(v_{f-w} > 0.0012)$ on η_D (x_D, θ_D). The solid lines in each plot represent the estimated values of ηs. To plot the solid lines, the mean value of other variables is used except for the main variable. Also, the dashed lines represent the standard deviation of the model error ($\pm\partial_A$). Also, the open circles represent the measured values of ηs.

Table 6. Ranges used for each Critical Factor

Critical factor (*y*-axis)	Main variable (*x*-axis)	Range (based on mean values of data)	
		***R*1**	***R*2**
$\eta_D(x_D, \theta_D)$	*AR*	$v_{f-w} \leq 0.0012$	$v_{f-w} > 0.0012$
$\eta_D(x_D, \theta_D)$	*UEI*	*SP/CNTs* ≤ 6.4	*SP/CNTs* > 6.4
$\eta_H(x_H, \theta_H)$	*t*	$\kappa \leq 0.1033$	$\kappa > 0.1033$
$\eta_M(x_M, \theta_M)$	*s/c ratio*	*w/c* ≤ 0.426	*w/c* > 0.426

Figs. 2 through 4 exhibit that most of the measured ηs are within $\pm\partial_A$ and they follow the similar trends as the estimated ηs. The good correlations between the measured and estimated values validate the applicability of the proposed critical factors to capture the mechanisms of CNTs affecting the flexural strength. As an example, comparing $R1$ and $R2$ in Fig. 3, it is obvious that the influence of t on the value of $\eta_H\ (x_H, \theta_H)$ becomes more pronounced at higher κ (see $R2$ in Fig. 3).

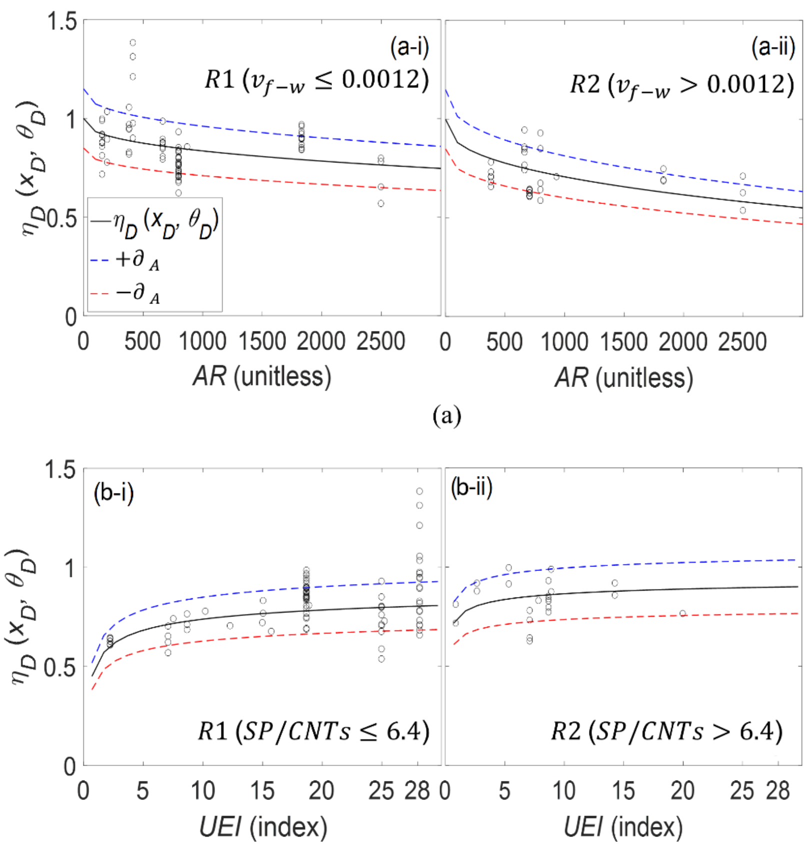

(a)

(b)

Fig. 2. Estimated vs. measured $\eta_D\ (x_D, \theta_D)$ as a function of: (a) *AR* and its interaction with v_{f-w} (b) *UEI* and its interaction with *SP/CNTs* ratio

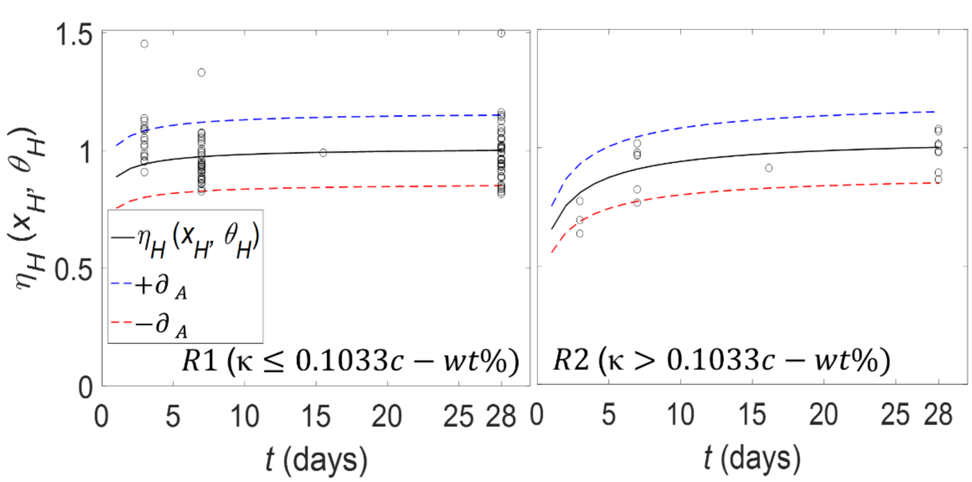

Fig. 3. Estimated vs. measured $\eta_H\ (x_H, \theta_H)$ as a function of t and its interaction with κ

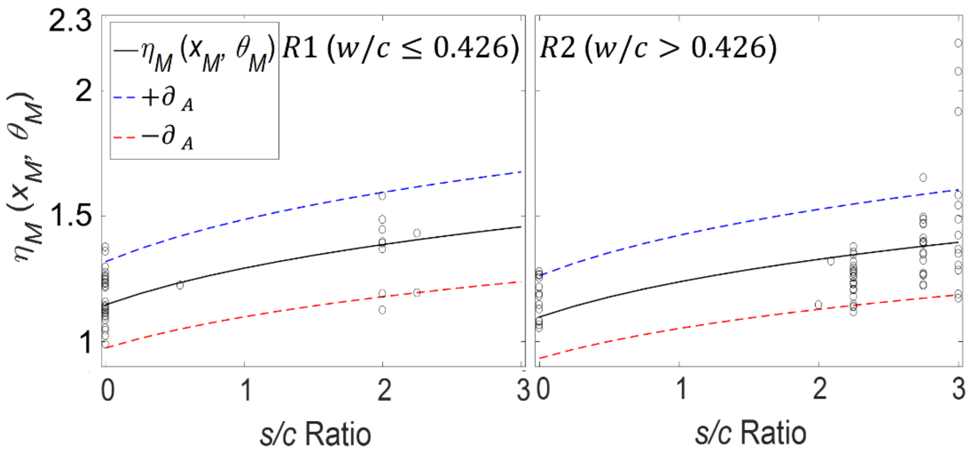

Fig. 4. Estimated vs. measured $\eta_M\ (x_M, \theta_M)$ as a function of *s/c* ratio and its interaction with *w/c* ratio

5.2. Model Selection Criteria

For model evaluation, it is assumed that there is a single correct model (or at least best model) that tradeoffs between goodness of fit and parsimony (i.e., preserves the model accuracy while using less variables). In this study, the two most commonly used penalized likelihood information criteria, Akaike information criterion (*AIC*) and Bayesian information criterion (*BIC*), are used to select the best model. The *AIC* and *BIC* can be calculated as follows:

$$AIC = -2\ log\ L(\mathbf{\Theta}) + 2N_p \tag{10}$$

$$BIC = -2\ log\ L(\mathbf{\Theta}) + N_p log N_s \tag{11}$$

where $log\ L(\mathbf{\Theta})$ is a measure of model fit, N_p is the number of unknown model parameters included in $\mathbf{\Theta}$, and N_s is the number of samples. The best model is selected from a set of candidate models containing different subsets of the critical factors as listed in Table 7. The best model is the one that neither under-fits nor over-fits (i.e., the model with the smallest approximated values of *AIC* and *BIC*). As seen in Table 7, Both *AIC* and *BIC* estimated values are smallest for model VIII compared with other competing models, indicating that including all critical factors is best to accurately predict the flexural strength.

Table 7. Model Selection Criteria (using random selection *A*: dataset I)

Model		N_p	Information criteria			*R*-squared
#	**Critical factors**		***AIC***	***BIC***	**Δ*AIC***	
I (Eq. (3))	Deterministic model	0	-18.73	-18.73	25.02	0.79
II	η_D	4	-8.014	-8.317	31.40	0.84
III	η_M	2	-11.15	-11.30	28.26	0.86
IV	η_H	1	-17.58	-17.66	21.83	0.87
V	$\eta_D \times \eta_M$	6	-6.434	-6.889	32.98	0.86
VI	$\eta_D \times \eta_H$	5	-11.80	-12.18	27.61	0.86
VII	$\eta_M \times \eta_H$	3	-16.43	-16.66	22.98	0.87
VIII (Eq. (8))	$\eta_D \times \eta_M \times \eta_H$	7	-39.41	-39.94	0	0.95

In addition, Δ*AIC* score which is defined as the difference between *AIC* values of the best model (AIC_{min}) and other competing models (AIC_i) are calculated:

$$\Delta AIC = AIC_i - AIC_{min} \tag{12}$$

According to Burnham and Anderson [51], the models with Δ*AIC* ≤ 2 have substantial evidence of better performance. The models with 4 ≤ Δ*AIC* ≤ 7 have less evidence and those models having Δ*AIC* > 10 have no evidence [51]. It can be seen that all competing models have Δ*AIC* value of greater than 10. This further confirm the superior performance of model VIII (Eq. (8)) compared with other candidate models.

6. Probability of Not Meeting Design Specifications

After calibrating the unknown model parameters using dataset I of random selection *A* (see Table 4), the probabilistic model (Eq. (8)) is used to identify the optimum ranges of each variable to maximize the flexural strength. This could be achieved by computing the probability of not meeting a specified flexural strength requirement (probability of failure).

Every structure has a capacity (*C*) and is subjected to some sort of demand (*D*) where both of them depend on random variables. Therefore, each of *C* and *D* has a probability distribution ($f_D(D)$ and $f_C(C)$) which could be combined to form a joint probability density function ($f_{CD}(C,D)$; see Fig. 5 (a)). If the joint probability density function is known, the probability of failure (P_f) could be easily determined by $P_f = \int_{-\infty}^{\infty}\int_{-\infty}^{C\leq D} f_{CD}(C,D)dC\, dD$. However, because of the large number of variables, the probability of failure cannot be determined in a mathematical way and therefore might be estimated using simulation-based analyses. Following the conventional notation in structural reliability theory [52], a limit state function $g(\cdot)$ is introduced such that the event $[g(\cdot) \leq 0]$ denotes the conditional probability of C not meeting D (i.e., $C - D < 0$; failure occurs). Conversely, if $C - D > 0$, the structure is safe.

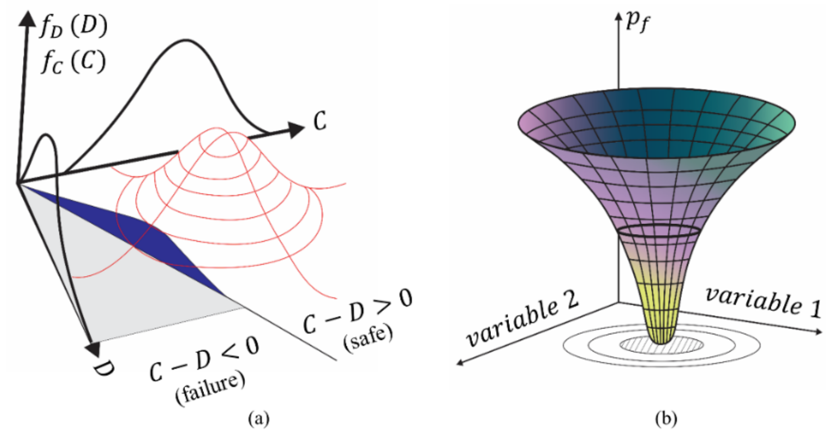

Fig. 5. Visualization of probability of failure: (a) joint probability density function (b) isoprobability lines

In this study, because there is no design criteria available in the literature, the minimum flexural strength requirement of CNT-cement composites is set to the deterministic value of 50% increase compared with the control specimen (i.e., D = 1.5 σ_m). Using the proposed probabilistic model in Eq. (8), the limit state function is formulated:

$$g(\alpha\sigma_m, x, \mathbf{\Theta}) = \sigma_c(\boldsymbol{x}, \mathbf{\Theta}) - \alpha\sigma_m \tag{13}$$

where α is the minimum flexural strength requirement (i.e., α = 1.5). Therefore, the probability of not meeting the demand is written as follows:

$$P(\mathbf{\Theta}) = P[g(\alpha\sigma_m, \boldsymbol{x}, \mathbf{\Theta}) \leq 0 \mid \mathbf{\Theta}] \tag{14}$$

where $P(\cdot \mid \cdot)$ represents the conditional probability of $g(\alpha\sigma_m, \boldsymbol{x}, \mathbf{\Theta}) \leq 0$ for given values of $\mathbf{\Theta}$.

Fig. 8 (b) visualizes the probability of failure using the isoprobability lines which connect pairs of values of different variables corresponding to the same probability of failure ($p[g(\alpha\sigma_m, \boldsymbol{x}, \boldsymbol{\Theta}) \leq 0]$). The lower values of probability of failure (P_f) indicates that the likelihood of $C - D > 0$ is higher (i.e., the flexural strength meets the design criteria).

6.1. Relationship between Variables Involved in Ultrasonication Procedure

Various dispersion techniques have been employed to uniformly disperse CNTs within the cement matrix; amongst which an ultrasonication procedure is the most common practice [5, 53].

Fig. 6 (a), (b) and (c) shows the contour plots of isoprobability lines for the ultrasonication energy indicator (UEI) versus κ, *AR* and *SP/CNTs* ratio, respectively, using the mean value of other variables.

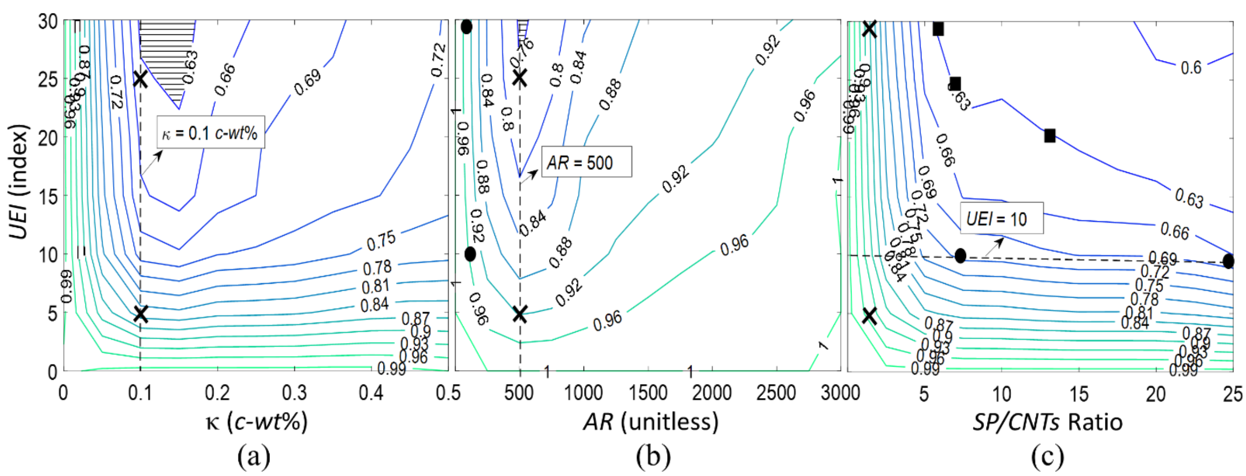

Fig. 6. Contour plots of the probability of failure as functions of (a) *UEI* and CNT concentration, (b) *UEI* and CNT aspect ratio (c) *UEI* and *SP/CNTs* ratio

Fig. 6 (a) shows that when using κ ≤ 0.05 *c-wt*%, the *UEI* has negligible impact on decreasing P_f. However, in case of a higher κ, the impact of *UEI* on P_f becomes more pronounced. For example, in case of κ = 0.1 *c-wt*% (based on weight percent of cement powder), increasing *UEI* from 5 to 25 results in 25% decrease in P_f from 0.85 to 0.64 (see crosses on the dashed line in Fig. 6 (a)). In addition, the P_f is lowest when incorporating UEI of above 25 and κ between 0.10 and 0.18 *c-wt*% (see the hatched area in Fig. 6 (a)).

Fig. 6 (b) shows as *AR* increases, the contribution of *UEI* to P_f becomes more pronounced. For example, in case of *AR* = 200, increasing *UEI* from 10 to 30 does not contribute to attaining lower P_f (see solid circles on the same probability of failure line ($P_f = 0.96$) in Fig. 6 (b)). However, in case of *AR* = 500, P_f decreases from 0.92 to 0.77 by increasing in *UEI* from 5 to 25 (see crosses on the dashed line in Fig. 6 (b)). Also, the lowest P_f is achieved when incorporating UEI of above 25 and *AR* of around 500 (see the hatched area in Fig. 6 (b)). Generally, as *UEI* increase, the circles which represent the isoprobability line of failure becomes smaller. This suggests that *UEI* is reaching to its threshold value.

Fig. 6 (c) shows that the impact of *UEI* on the P_f increases as *SP/CNTs* ratio increases. Generally, as *SP/CNTs* ratio increases, lower *UEI* is needed to attain the same P_f. For example, incorporating UEI and *SP/CNTs* ratio of 30 and 6, respectively, exhibits the same P_f as utilizing *UEI* and *SP/CNTs* ratio of 25 and 7 or 20 and 12, respectively, does (see the solid squares on the same probability of failure line ($P_f = 0.63$) in Fig. 6 (c)). Besides, in case of a constant *UEI*, the probability of failure is not changed by increasing in *SP/CNTs* ratio beyond a certain limit. For example, in case of *UEI* = 10, the P_f reaches a constant value of around 0.7 beyond *SP/CNTs* ratio of approximately 7 (see solid circles on the dashed line in Fig. 6 (c)) and this threshold reaches sooner in lower *UEI* values. This might be explained by the better dispersibility of CNTs using higher *UEI*. Thereafter, higher amount of *SP* could be taken by CNTs to wet their surface [54]. Conversely, in the case of *SP/CNTs* ratio of below 3, higher amount of *UEI* does not contribute to lowering the P_f (see crosses on the same P_f line of 0.96 in Fig. 6 (c)).

6.2. Relationship between *w/c* and *s/c* Ratios

Fig. 7 shows the contour plot of the probability of failure lines as a function of *s/c* and *w/c* ratios. The probability of failure decreases as s/c ratio increases. For example, in case of a constant *w/c* = 0.45, increasing *s/c* ratio from 0 (i.e., cement paste) to 3 results in decreasing the P_f from 0.93 to 0.84 (see the solid squares on the dash-dotted line in Fig. 7). Conversely, P_f increases as *w/c* ratio increases. For example, in case of a constant *s/c* ratio of 2, the P_f increases from 0.79 to 0.95 as the *w/c* ratio increases from 0.35 to 0.60 (see the solid circles on the dashed line in Fig. 7). Also, there are several options to attain the same P_f using certain combinations of *w/c* and *s/c* ratios. For example, P_f = 0.80 can be attained when using *w/c* and *s/c* ratios of 0.40 and 3 or 0.35 and 2, respectively (see crosses on the same P_f line of 0.8 in Fig. 7).

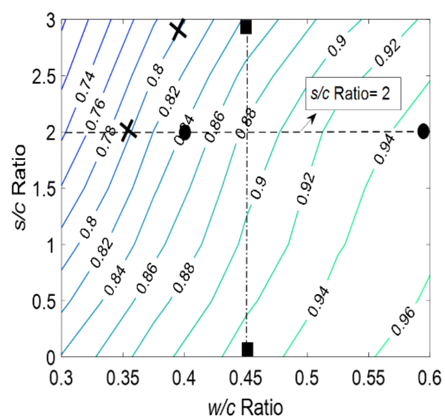

Fig. 7. Contour plot of probability of failure as a function of *w/c* and *s/c* ratios

6.3. Relationship between κ and *t*

Fig. 8 shows the influences of κ and *t* on P_f. In case of κ ≤ 0.05 *c-wt*%, the influence of *t* on P_f is negligible. For example, when κ = 0.05 *c-wt*% (see dashed line in Fig. 8), P_f is not affected by the variation in *t* from 10 to 28 days (see the solid circles on the same probability of failure line of P_f = 0.78 in Fig. 8). The contribution of *t* to P_f increases as κ increases. The same P_f can be achieved using certain combinations of κ and *t*. For example, when κ = 0.1 *c-wt*%, P_f reaches 0.66

at 14 days, while 25 days is needed to attain the same P_f at κ = 0.4 *c-wt*% (see crosses on the same probability of failure line in Fig. 8).

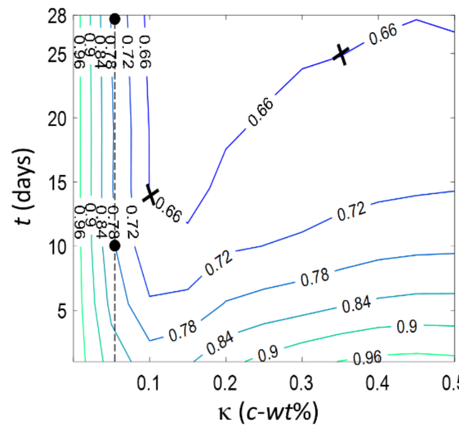

Fig. 8. Contour plot of probability of failure as a function of CNT concentration and hydration age

6.4. Influence of Optimum Ranges of Variables on Probability of Failure

Fig. 9 shows contour plots of probability of failure as a function of κ and *AR*. Fig. 9 (a) and (b) show the isoprobability lines for flexural strength requirement of at least 50% increase compared to the control (i.e., $D = 1.5\ \sigma_m$) when using mean and optimum values of other variables, respectively. The optimum values of variables (*UEI* = 30, *SP/CNTs* = 6, *w/c* = 0.4, and *s/c* = 3) is obtained using the lowest P_f in Figs. 6 (c) and 7.

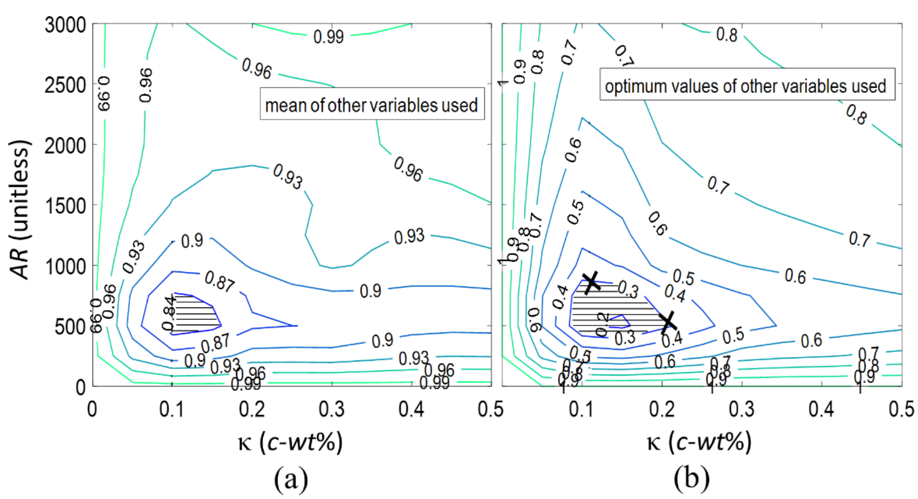

Fig. 9. Contour plots of probability of failure as a function of CNT concentration and aspect ratio using (a) mean of other variables (b) optimum values of other variables

Generally, P_f decreases as κ or *AR* increases up to their optimum values, beyond which P_f increases. Also, In case of κ ≤ 0.05 *c-wt*%, the impact of *AR* on P_f is minimal. Besides, in case of *AR* ≤ 500, the impact of κ on P_f is negligible.

Fig. 9 (a) shows that P_f is lowest ($P_f = 0.84$) when using *AR* ranging from 400 to 800 and κ between 0.08 and 0.18 *c-wt*% (see hatched areas in Fig. 9 (a)). Comparing Fig. 9 (a) and (b), it is seen that incorporating optimum values of other variables significantly contribute to decreasing P_f by 64% from 0.84 to 0.30. Besides, the same P_f can be attained when using CNTs having either lower κ with higher *AR* or higher κ with lower *AR*. For example, the probability of failure is 0.3 in case of using *AR* = 800 with κ = 0.1 *c-wt*% or *AR* = 500 with κ = 0.2 *c-wt*% (see crosses on the same P_f line of 0.3 in Fig. 9(b)).

7. Sensitivity and Importance Analyses

This section presents the sensitivity and importance analyses for different variables in the limit state function (Eq. (13)) to assess their effect on the probability estimates, helping researchers to minimize P_f by designing more efficiently.

7.1. Sensitivity Analysis

The sensitivity analysis is used to determine which variables are most sensitive to the change of P_f [55]. To compute the sensitivity measures of different variables, the vector **δ** is used:

$$\boldsymbol{\delta} = \boldsymbol{\sigma}\boldsymbol{\nabla}_{\boldsymbol{\Theta}_f}\beta \tag{15}$$

where $\boldsymbol{\sigma}$ is diagonal matrix with diagonal elements given by the standard deviation of each random variable in $\boldsymbol{x}$, β is a reliability index from first order reliability method (FORM) analysis, and $\boldsymbol{\nabla}_{\boldsymbol{\Theta}_f}\beta$ is a gradient vector of β with respect to $\boldsymbol{\Theta}_f$ computed at the mean point. The sensitivity measures can be employed for optimal design and to gain insights into which variable(s) to change in order to increase the flexural strength.

The sensitivity measure of each variable is computed with respect to three main variables: κ, *AR*, and *UEI*. These variables are believed to have the highest impact on the flexural strength of CNT-cement nanocomposites. Fig. 10 shows the sensitivity measure of each variable as a function of κ (see Fig. 10 (a)), *AR* (see Fig. 10 (b)) and *UEI* (see Fig. 10 (c)) while incorporating mean values of other variables. The higher change in the sensitivity measure of each variable (y-axis) with respect to the changes of x-axis (i.e., main variable) indicates the higher sensitivity of P_f to the change in that variable (for D = 1.5 σ_m).

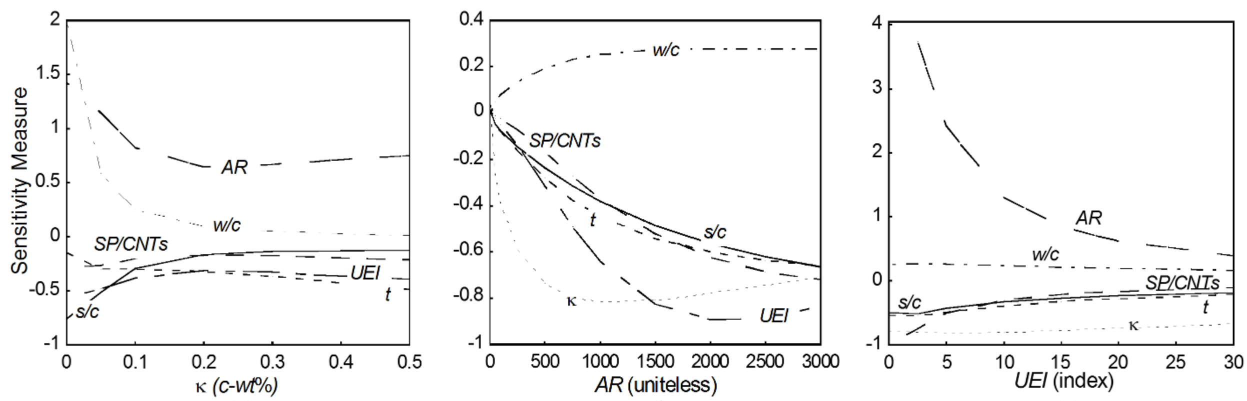

(a) (b) (c)

Fig. 10. Sensitivity measures for flexural strength as functions of (a) κ (b) *AR* (c) *UEI*

Fig. 10 (a) shows that up to κ = 0.2 *c-wt*%, the sensitivity measure of most variables changes significantly. However, the sensitivity measure remains almost constant beyond κ = 0.2 *c-wt*%. In case of κ ≤ 0.2 *c-wt*%, *w/c* ratio, *AR* and *s/c* ratio are the most sensitive variables to the changes in P_f, respectively, while *SP/CNTs* ratio and *t* are the least sensitive parameters. In case of κ > 0.2 *c-wt*%, P_f is most sensitive to the variation in *t* followed by *AR*. When computing the sensitivity measures as a function of *AR* (see Fig. 10 (b)), κ is the most sensitive parameter below *AR* of around 500 beyond which the sensitivity of κ to change the P_f gradually decreases. In contrast *w/c* ratio is the least sensitive parameter to the change in P_f. When computing the sensitivity measure with respect to the change in *UEI* (see Fig. 10 (c)), *AR* and *SP/CNTs* ratio are the most sensitive parameters to the changes in P_f.

In addition, the negative or positive value of the sensitivity measure for each variable indicates that P_f decreases or increases, respectively, as the amount of that variable increases. For example, the positive values of sensitivity measure for *AR* and/or *w/c* ratio indicates that the probability of failure increases as the value of *AR* and/or *w/c* ratio increases. On the other hand, Fig. 10 (a) shows that P_f decreases (i.e., the chance of attaining at least 50% increase in the flexural strength increases) as the value of *t*, *UEI*, *s/c* ratio, and *SP/CNTs* ratio increases. Fig 10 (c) shows that as *UEI* increases, the sensitivity measure of *AR* gets closer to zero, indicating that higher *AR* is beneficial to increase the flexural strength in case of a high *UEI* (i.e., proper CNT dispersion).

7.2. Importance Analysis

In the limit state function (Eq. (13)), some variables have larger impacts on the variance of the limit state function and some variables have smaller impacts, and therefore are less important. The vector of importance measures ($\boldsymbol{\gamma}$) is computed as follows [56]:

$$\boldsymbol{\gamma}^T = \frac{\boldsymbol{\alpha}^T \boldsymbol{J}_{\boldsymbol{u}^*\boldsymbol{z}^*} \boldsymbol{SD}'}{\|\boldsymbol{\alpha}^T \boldsymbol{J}_{\boldsymbol{u}^*\boldsymbol{z}^*} \boldsymbol{SD}'\|} \tag{16}$$

where $\boldsymbol{\alpha}$ is row vector of the negative normalized gradient of the limit state function evaluated at the design point in standard normal space, $\boldsymbol{z}$ is vector of random variables ($\boldsymbol{z} = (x_p, \boldsymbol{\Theta})$), $\boldsymbol{J}_{\boldsymbol{u}^*\boldsymbol{z}^*}$ is Jacobian of the probability transformation from the original space (i.e., $\boldsymbol{z}$) to the standard normal space (i.e., $\boldsymbol{u}$) with respect to the coordinates of the most likely failure point (i.e., design point, $\boldsymbol{z}^*$) and $\boldsymbol{SD}'$ is the standard deviation diagonal matrix of equivalent normal variables $\boldsymbol{z}'$ defined by the linearized inverse transformation $\boldsymbol{z}' = \boldsymbol{z}^* + \boldsymbol{J}_{\boldsymbol{z}^*\boldsymbol{u}^*}(\boldsymbol{u} - \boldsymbol{u}^*)$ at the design point. The elements in the matrix $\boldsymbol{SD'}$ are the square root of the corresponding diagonal elements of the covariance matrix $\Sigma' = \boldsymbol{J}_{\boldsymbol{z}^*\boldsymbol{u}^*}\boldsymbol{J}_{\boldsymbol{z}^*\boldsymbol{u}^*}^T$ of the variables in the $\boldsymbol{z'}$.

The importance measure is used to rank the importance of different variables on the variability of the limit state function with respect to κ (see Fig. 11 (a)), *AR* (see Fig. 11 (b)) and *UEI* (see Fig. 11 (c)) when using mean values of other variables. In importance analysis, the higher absolute value of the importance measure vector ($\boldsymbol{\gamma}$) for each variable indicates the higher importance of that variable.

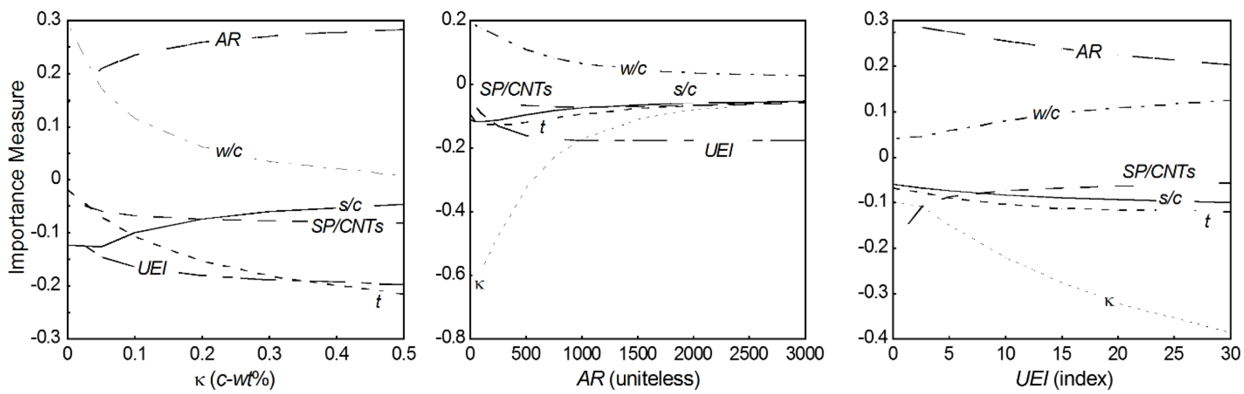

Fig. 11. Importance measure for flexural strength as functions of (a) κ (b) *AR* (c) *UEI*

Fig. 11 (a) shows that *w/c* ratio is the most important variable at κ ≤ 0.05 *c-wt*%. The importance of *w/c* ratio gradually decreases as κ increases and beyond κ = 0.3 *c-wt*%, the *w/c* ratio is the least important variable to the variation in the limit state function (the smallest absolute value of importance measure (y-axis) amongst other variables). As κ increases, the importance of *AR*, *t* and *UEI* also increases, while the importance of *SP/CNTs* ratio remains almost constant. For example, *t* is the least important variable at κ < 0.05 *c-wt*%. However, at κ = 0.5 *c-wt*%, *t* is the second most important variable after *AR*.

Fig. 10 (b) shows that as *AR* increases, the importance of κ decreases. Below *AR* of around 1000, κ is the most important variable to the change in P_f. However, beyond *AR* of 2500, κ is the least important variable to the change of the flexural strength.

Fig. 10 (c) shows that when *UEI* < 5, *AR* and *SP/CNTs* ratio are the most important variables to the change in the flexural strength, respectively. However, the importance of *SP/CNTs* ratio decreases by increasing in *UEI* and it becomes the least important variable at *UEI* > 10. In addition, as *UEI* increases, the importance of κ and *w/c* ratio increases. When *UEI* ≥ 15, κ is the most important variable to the variance of the limit state function.

8. Conclusions

This paper proposes a bias-free probabilistic model based on the available deterministic Kelly-Tyson model to predict the flexural strength of CNT-cement nanocomposites (pastes and mortars). The proposed model considers the influences of CNT physical properties, dispersion state, matrix composition and cement hydration using a Bayesian approach. The information obtained from the probabilistic model provides better understanding of the mechanisms of CNTs improving the flexural strength, leading to more efficient designs. The following conclusions can be made:

1. The proposed probabilistic model is able to predict the flexural strength within 15% error of the experimental test data. In addition, the proposed model can be updated if new data becomes available in the future, leading to more accurate predictions.
2. Up to certain limits, the higher CNT aspect ratio (*AR*) results in superior improvement in the flexural strength. Generally, *AR* ranging from 400 to 800 and concentration (κ) ranging between 0.08 and 0.18 *c-wt*% (based on weight percent of cement powder) results in the highest improvement of the flexural strength.

3. There are several options to achieve comparable improvements in the flexural strength with varied combinations of the influential variables. For example, when using mean of other variables, utilizing *w/c* and *s/c* ratios of 0.4 and 3 or 0.35 and 2, respectively, results in similar improvements of the flexural strength.
4. The *AR*, *w/c* ratio and *s/c* ratio are the most sensitive variables to the change in the flexural strength with respect to κ. Also, *AR* and *SP/CNTs* ratio are the two most important variables with respect to *UEI*. As κ increases, the importance of *AR* and age of specimen increases, while the importance of *w/c* and *s/c* ratios decreases. In addition, as *UEI* increase, the importance of *SP/CNTs* ratio to attain the superior flexural strength decreases.

References

1. Al-Hadithi, A.I., A.T. Noaman, and W.K. Mosleh, *Mechanical properties and impact behavior of PET fiber reinforced self-compacting concrete (SCC).* Composite Structures, 2019. **224**: p. 111021.
2. Yoo, D.-Y., S.-T. Kang, and Y.-S. Yoon, *Enhancing the flexural performance of ultra-high-performance concrete using long steel fibers.* Composite Structures, 2016. **147**: p. 220-230.
3. Balaguru, P.N. and S.P. Shah, *Fiber-reinforced cement composites*. 1992: McGraw-Hill Inc.,. 530.
4. Bentur, A. and S. Mindess, *Fibre reinforced cementitious composites*. 2006: Taylor & Francis,. 601.
5. Ramezani, M., Y.H. Kim, and Z. Sun, *Mechanical Properties of Carbon Nanotube Reinforced Cementitious Materials: Database and Statistical Analysis.* Magazine of Concrete Research, 2019: p. 1-62.
6. Konsta-Gdoutos, M.S., et al., *Fresh and mechanical properties, and strain sensing of nanomodified cement mortars: The effects of MWCNT aspect ratio, density and functionalization.* Cement and Concrete Composites, 2017. **82**: p. 137-151.
7. Gdoutos, E.E., M.S. Konsta-Gdoutos, and P.A. Danoglidis, *Portland cement mortar nanocomposites at low carbon nanotube and carbon nanofiber content: A fracture mechanics experimental study.* Cement and Concrete Composites, 2016. **70**: p. 110-118.
8. Demczyk, B.G., et al., *Direct mechanical measurement of the tensile strength and elastic modulus of multiwalled carbon nanotubes.* Materials Science and Engineering: A, 2002. **334**(1): p. 173-178.
9. Thostenson, E.T. and T.-W. Chou, *On the elastic properties of carbon nanotube-based composites: modelling and characterization.* Journal of Physics D: Applied Physics, 2003. **36**(5): p. 573.
10. Konsta-Gdoutos, M.S., Z.S. Metaxa, and S.P. Shah, *Highly dispersed carbon nanotube reinforced cement based materials.* Cement and Concrete Research, 2010. **40**(7): p. 1052-1059.
11. Danoglidis, P.A., et al., *Strength, energy absorption capability and self-sensing properties of multifunctional carbon nanotube reinforced mortars.* Construction and Building Materials, 2016. **120**: p. 265-274.
12. Sadeghi-Nik, A., et al., *Modification of microstructure and mechanical properties of cement by nanoparticles through a sustainable development approach.* Construction and Building Materials, 2017. **155**: p. 880-891.
13. Kafi, M.A., et al., *Microstructural characterization and mechanical properties of cementitious mortar containing montmorillonite nanoparticles.* Journal of Materials in Civil Engineering, 2016. **28**(12): p. 04016155.
14. Ramezani, M., Y.H. Kim, and Z. Sun, *Modeling the Mechanical Properties of Cementitious Materials Containing CNTs* Cement and Concrete Composites, 2019: p. 103347.
15. Chen, B., et al., *Length effect of carbon nanotubes on the strengthening mechanisms in metal matrix composites.* Acta Materialia, 2017. **140**: p. 317-325.
16. Zare, Y., *Effects of interphase on tensile strength of polymer/CNT nanocomposites by Kelly–Tyson theory.* Mechanics of Materials, 2015. **85**: p. 1-6.
17. Bakshi, S.R. and A. Agarwal, *An analysis of the factors affecting strengthening in carbon nanotube reinforced aluminum composites.* Carbon, 2011. **49**(2): p. 533-544.
18. Fu, S.-Y., et al., *Effects of particle size, particle/matrix interface adhesion and particle loading on mechanical properties of particulate–polymer composites.* Composites Part B: Engineering, 2008. **39**(6): p. 933-961.
19. Halpin, J. and J. Kardos, *The Halpin-Tsai equations: a review.* Polymer Engineering & Science, 1976. **16**(5): p. 344-352.

20. Kelly, A. and a.W. Tyson, *Tensile properties of fibre-reinforced metals: copper/tungsten and copper/molybdenum.* Journal of the Mechanics and Physics of Solids, 1965. **13**(6): p. 329-350.
21. Ayatollahi, M., et al., *Effect of multi-walled carbon nanotube aspect ratio on mechanical and electrical properties of epoxy-based nanocomposites.* Polymer Testing, 2011. **30**(5): p. 548-556.
22. Yeh, M.-K., N.-H. Tai, and J.-H. Liu, *Mechanical behavior of phenolic-based composites reinforced with multi-walled carbon nanotubes.* Carbon, 2006. **44**(1): p. 1-9.
23. Montazeri, A., et al., *Mechanical properties of multi-walled carbon nanotube/epoxy composites.* Materials & Design, 2010. **31**(9): p. 4202-4208.
24. Navidfar, A. and L. Trabzon, *Graphene type dependence of carbon nanotubes/graphene nanoplatelets polyurethane hybrid nanocomposites: Micromechanical modeling and mechanical properties.* Composites Part B: Engineering, 2019. **176**: p. 107337.
25. Kurita, H., et al., *Load-bearing contribution of multi-walled carbon nanotubes on tensile response of aluminum.* Composites Part A: Applied Science and Manufacturing, 2015. **68**: p. 133-139.
26. Liao, J.-z., M.-J. Tan, and I. Sridhar, *Spark plasma sintered multi-wall carbon nanotube reinforced aluminum matrix composites.* Materials & Design, 2010. **31**: p. S96-S100.
27. Lachman, N., et al., *Interfacial load transfer in carbon nanotube/ceramic microfiber hybrid polymer composites.* Composites Science and Technology, 2012. **72**(12): p. 1416-1422.
28. Shokrieh, M.M. and R. Rafiee, *Investigation of nanotube length effect on the reinforcement efficiency in carbon nanotube based composites.* Composite Structures, 2010. **92**(10): p. 2415-2420.
29. Swamy, R. and P. Mangat, *A theory for the flexural strength of steel fiber reinforced concrete.* Cement and Concrete Research, 1974. **4**(2): p. 313-325.
30. Tassew, S. and A. Lubell, *Mechanical properties of glass fiber reinforced ceramic concrete.* Construction and Building Materials, 2014. **51**: p. 215-224.
31. Agarwal, B.D., L.J. Broutman, and K. Chandrashekhara, *Analysis and performance of fiber composites*. 2017: John Wiley & Sons.
32. Krenchel, H., *Fibre reinforcement; theoretical and practical investigations of the elasticity and strength of fibre-reinforced materials.* 1964.
33. Rosenthal, J., *A model for determining fiber reinforcement efficiencies and fiber orientation in polymer composites.* Polymer composites, 1992. **13**(6): p. 462-466.
34. Brown, J., et al., *Delamination Mechanics of Carbon Nanotube Micropillars.* ACS applied materials & interfaces, 2019. **11**(38): p. 35221-35227.
35. Pukanszky, B., *Influence of interface interaction on the ultimate tensile properties of polymer composites.* Composites, 1990. **21**(3): p. 255-262.
36. Zare, Y., et al., *An analysis of interfacial adhesion in nanocomposites from recycled polymers.* Computational Materials Science, 2014. **81**: p. 612-616.
37. Bilotti, E., et al., *Sepiolite needle-like clay for PA6 nanocomposites: an alternative to layered silicates?* Composites Science and Technology, 2009. **69**(15-16): p. 2587-2595.
38. Lazzeri, A. and V.T. Phuong, *Dependence of the Pukánszky's interaction parameter B on the interface shear strength (IFSS) of nanofiller-and short fiber-reinforced polymer composites.* Composites Science and Technology, 2014. **93**: p. 106-113.
39. Gardoni, P., A.D. Kiureghian, and K.M. Mosalam, *Probabilistic Capacity Models and Fragility Estimates for Reinforced Concrete Columns based on Experimental Observations.* Journal of Engineering Mechanics, 2002. **128**(10): p. 1024-1038.
40. Box, G.E. and G.C. Tiao, *Bayesian inference in statistical analysis*. Vol. 40. 2011: John Wiley & Sons.
41. Gardoni, P., D. Trejo, and Y.H. Kim, *Time-Variant Strength Capacity Model for GFRP Bars Embedded in Concrete.* Journal of Engineering Mechanics, 2013. **139**(10): p. 1435-1445.

42. Stynoski, P., P. Mondal, and C. Marsh, *Effects of silica additives on fracture properties of carbon nanotube and carbon fiber reinforced Portland cement mortar.* Cement and Concrete Composites, 2015. **55**: p. 232-240.
43. Zou, B., et al., *Effect of ultrasonication energy on engineering properties of carbon nanotube reinforced cement pastes.* Carbon, 2015. **85**: p. 212-220.
44. Metaxa, Z.S., et al., *Highly concentrated carbon nanotube admixture for nano-fiber reinforced cementitious materials.* Cement and Concrete Composites, 2012. **34**(5): p. 612-617.
45. Danoglidis, P.A., et al., *MWCNT and CNF Cementitious Nanocomposites for Enhanced Strength and Toughness.* Mechanics of Composite and Multi-functional Materials, 2016. **7**: p. 241-246.
46. Gdoutos, E.E., et al., *Advanced cement based nanocomposites reinforced with MWCNTs and CNFs.* Frontiers of Structural and Civil Engineering, 2016. **10**(2): p. 142-149.
47. Konsta-Gdoutos, M.S., Z.S. Metaxa, and S.P. Shah, *Multi-scale mechanical and fracture characteristics and early-age strain capacity of high performance carbon nanotube/cement nanocomposites.* Cement and Concrete Composites, 2010. **32**(2): p. 110-115.
48. Ramezani, M., *Design and predicting performance of carbon nanotube reinforced cementitious materials: mechanical properties and dipersion characteristics*. Electronic Theses and Dissertations, 2019. Paper 3255.
49. Weiss, S.M. and C.A. Kulikowski, *Computer systems that learn: classification and prediction methods from statistics, neural nets, machine learning, and expert systems*. 1991: Morgan Kaufmann Publishers Inc.
50. Kim, Y.H., Y. Park, and J.-W. Bai, *Probabilistic Shear Capacity Models for Concrete Members with Internal Composite Reinforcement.* Journal of Composites for Construction, 2016. **21**(2): p. 04016083.
51. Burnham, K.P. and D.R. Anderson, *Multimodel inference: understanding AIC and BIC in model selection.* Sociological methods & research, 2004. **33**(2): p. 261-304.
52. Ditlevsen, O. and H.O. Madsen, *Structural reliability methods*. Vol. 178. 1996: Wiley New York.
53. Ramezani, M., et al. *Influence of Carbon Nanotubes on SCC Flowability*. in *8th International RILEM Symposium on Self-Compacting Concrete*. 2016. Washington DC, USA.
54. Strano, M.S., et al., *The role of surfactant adsorption during ultrasonication in the dispersion of single-walled carbon nanotubes.* Journal of Nanoscience and Nanotechnology, 2003. **3**(1-2): p. 81-86.
55. Hohenbichler, M. and R. Rackwitz, *Sensitivity and importance measures in structural reliability.* Civil Engineering Systems, 1986. **3**(4): p. 203-209.
56. Der Kiureghian, A. and J. Ke. *Finite-element based reliability analysis of frame structures*. in *Proc. 4th Int. Conference on Structural Safety and Reliability*. 1985.